Timing Analysis of Light Curves in the Tartarus Active Galactic Nuclei Database

Paul M. O'Neill*, Kirpal Nandra*, Iossif E. Papadakis†** and T. Jane Turner‡§

*Astrophysics Group, Imperial College London, Blackett Laboratory, Prince Consort Road, London SW7 2AW, United Kingdom
†Department of Physics, University of Crete, 71 003, Heraklion, Crete, Greece
**IESL, FORTH-Hellas, 71 110, Heraklion, Crete, Greece
‡Laboratory for High Energy Astrophysics, Code 660, NASA Goddard Space Flight Center, Greenbelt, MD 20771
§University of Maryland, Baltimore County, 1000 Hilltop Circle, Baltimore, MD 21250

Abstract.
The Tartarus database contains products for 529 *ASCA* observations of active galactic nuclei. We have been updating Tartarus to include observing sequences conducted after 1999 January. The revised database will contain products for 375 objects, with a total of 614 observing sequences. We have begun a systematic timing analysis of the Tartarus light curves. We present here some preliminary results of an investigation into the relation between excess variance and black-hole mass. Having optimised our analysis to minimize the scatter in the variance measurements, we find that the narrow-line active galactic nuclei follow roughly the same relation as the broad-line objects.

X-RAY VARIABILITY IN ACTIVE GALACTIC NUCLEI

The existence of variability in the X-ray emission from active galactic nuclei (AGNs), on time-scales of days to years, was established roughly three-decades ago [e.g. 1, and references therein]. Variations on time-scales shorter than this are also common. The launch of *EXOSAT*, with its long orbit, meant that well-sampled X-ray light curves could be obtained for time-scales of minutes to days. The power-spectra generated from *EXOSAT* light curves could be described by an unbroken power-law [e.g. 2, 3]. Archival observations spanning weeks to months showed that, for two objects, the power-law flattened at low frequencies [4, 5]. More recently, *RXTE* and *XMM-Newton* observations have shown that the power-spectra of AGN light curves exhibit broken power-law shapes very similar to those seen in galactic black-hole X-ray binaries [e.g. 6, 7].

As well as power-spectral density, the *excess variance* can be used to characterise the X-ray variability [e.g. 8]. Excess variance is defined as the variance in the light curve in excess of the statistical fluctutations. The window function affects the excess variance less than it does the power-spectral density. Therefore, the excess variance is a useful quantity for the description of light curves containing many gaps.

An anti-correlation was found between excess variance and luminosity for a sample of AGNs observed by the *Advanced Satellite for Cosmology and Astrophysics* (*ASCA*) [8]. Later work using *ASCA* data found that, for a given luminosity, the X-ray light curves of narrow-line Seyfert 1 (NLS1) galaxies exhibit a larger excess variance than broad-line Seyfert 1 (BLS1) galaxies [9, 10]. This result can be explained if, for a given luminosity, the NLS1s have a lower black-hole mass than the BLS1s. A lower mass results in faster variations, and this is seen as a larger excess variance. Alternatively, other properties of the variability, not just the time-scale, might differ between NLS1s and BLS1s. These alternatives can be tested through examining the dependence of the excess variance on black-hole mass.

The relationship between excess variance and black-hole mass, for Seyfert 1 galaxies and quasi-stellar objects (QSOs), has been studied using *ASCA* data (time-scale $\sim$ 1 d) [11, 12]. These studies revealed an anti-correlation between mass and variance. Moreover, the narrow-line (NL AGNs) and broad-line (BL AGNs) objects followed the same relation. This relation could be explained if the power-spectrum is an unbroken power-law [$P(\nu) \propto \nu^{-\alpha}$] with $\alpha \sim 2$ [11].

An investigation using *RXTE* data (time-scale $\sim$ 300 d) presents a different picture [13]. The BLS1s, and the NLS1 MCG–6-3-15, follow a variance–mass rela-

tion that is consistent with a universal power-spectral shape. This 'average' spectrum comprises a twice-broken power-law which breaks from $\alpha = 0$ to 1 at the so-called 'low-frequency break', and from $\alpha = 1$ to 2 at the 'high-frequency break'. The break frequencies are inversely proportional to black-hole mass, and the amplitude, when represented in power$\times$frequency space, is constant. This power-spectral shape resembles that seen in the black-hole binary Cyg X-1 in the low/hard state. The other NLS1 in the sample, NGC 4051, *did not* follow the above relation. The excess variance of NGC 4051 was consistent with a singly-broken power-law, breaking from $\alpha = 1$ to 2, with a break frequency that is 20 times higher than for BLS1s. This shape is similar to that seen in Cyg X-1 in the high/soft state. An analysis of *RXTE* (time-scale $\sim$ 6.5 years) and *XMM-Newton* (time-scale $\sim$ 100 ks) data on NGC 4051 revealed a high/soft state power-spectral shape [6]. Moreover, in plots of high-frequency break versus black-hole mass, the NLS1s were found to have systematically higher break frequencies than the BLS1s [13, 6].

The excess variance versus luminosity relation for the BLS1 galaxies can be explained as a consequence of the variance-mass relation if the BLS1s radiate at $\sim$ 13 per cent of the Eddington luminosity [13]. The location of NGC 4051 in the variance-luminosity plane is consistent with that object radiating at $\sim$ 10 per cent Eddington [13].

These results from *RXTE* and *XMM-Newton* suggest that the power-spectral properties of AGN depend on black-hole mass *and* at least one other parameter. The dependence with mass is perhaps the least surprising, since we expect the size of the emission region—and, therefore, the variability time-scale—to scale with mass. A useful step forward, then, is to account for this mass dependence and investigate how the X-ray variability depends on other parameters. This is best achieved through maximizing the sample size and minimizing observational scatter.

TARTARUS: A DATABASE OF ASCA OBSERVATIONS OF AGN

The *ASCA* satellite was launched into a 96 minute orbit on 1993 February 20 and ceased observing on 2000 July 14 [14][1]. The satellite comprised four X-ray telescopes and four corresponding focal-plane instruments [15]. There were two solid-state imaging spectrometers (SIS0 and SIS1) [16] and two gas imaging spectrometers (GIS2 and GIS3) [17]. The effective energy ranges were 0.5–10 keV and 0.7–10 keV for the SIS and GIS instruments, respectively.

The Tartarus database contains products for all *ASCA* observations with targets designated as AGN [18]. The products comprise SIS and GIS event files, images, spectra, and light curves. Version 2 is presently available[2] at Goddard Space Flight Centre (GSFC), and consists of 529 observing sequences. We are updating and improving the database to include data collected after 1999 January. The revised database will consist of 614 sequences with a total of 375 objects. Version 3 of Tartarus is to be made available at GSFC and Imperial College London.

We are conducting a systematic timing analysis of the light curves in the Tartarus database. Tartarus is well suited to such a project because it contains data for a large sample of objects. The overall aim of the project is to uncover any correlations that exist between the properties of the X-ray variability and other parameters.

We have begun the project by investigating those AGN for which the black-hole mass has been estimated. We present here some preliminary results of an investigation between excess variance and black-hole mass. Our work is similar to that conducted using *RXTE* data as described in the previous section.

ANALYSIS

We restricted our analysis to narrow- and broad-line AGN. Our sample contains Seyfert 1 galaxies and QSOs. We do not differentiate between Seyfert galaxies and QSOs, but we shall simply refer to each object as either a narrow- or broad-line AGN [12]. We used the 'rms spectrum' [24] reverberation-mapping mass estimate if available, otherwise we used the mass estimate determined from the optical luminosity [e.g 23]. The objects in our sample, along with their black-hole masses, are listed in Table 1. The mass measurements with no error bars were estimated via the optical luminosity. The uncertainty in these measurements is about 0.5 dex [12]. Objects with Hβ $<$ 2000 km s^{-1} were classified as NL AGNs [9, 12, 25, 26].

The variance in a light curve is equal to the integral of the power-spectral density between the frequency limits set by the time resolution and duration of the light curve. Therefore, the use of different binnings and durations per object will introduce artificial scatter. We wish to minimize this scatter. Therefore, we used a time resolution of 256 s for all light curves, and restricted them to be between 30 and 40 ks in duration.

[1] see also `http://heasarc.gsfc.nasa.gov/docs/asca/ascagof.html`

[2] `http//:tartarus.gsfc.nasa.gov`

TABLE 1. Name, type and black-hole mass for each object having at least 1 valid Tartarus light curve. The objects exhibiting significant variability are listed first.

Object Name	Type	Mass (10^7 $M_\odot$)	Ref.
Variable			
NGC 4051	NL AGN	$0.05^{+0.06}_{-0.03}$	[19]
MRK 766	NL AGN	0.0832	[12]
AKN 564	NL AGN	0.115	[12]
MCG−6-3-15	NL AGN	0.155	[12]
MRK 1040	BL AGN	0.229	[12]
NGC 4593	BL AGN	0.66 ± 0.52	[20]
NGC 7469	BL AGN	$0.75^{+0.74}_{-0.75}$	[21]
MRK 110	NL AGN	$0.77^{+0.28}_{-0.29}$	[21]
NGC 3783	BL AGN	0.87 ± 0.11	[22]
MRK 290	BL AGN	1.12	[12]
NGC 4151	BL AGN	$1.20^{+0.83}_{-0.70}$	[21]
TON S180	NL AGN	1.23	[12]
NGC 3516	BL AGN	1.68 ± 0.33	[20]
NGC 3227	BL AGN	3.6 ± 1.4	[20]
MRK 509	BL AGN	9.2 ± 1.1	[21]
NGC 5548	BL AGN	$9.4^{+1.7}_{-1.4}$	[21]
Non-Variable			
MRK 335	NL AGN	$0.38^{+0.14}_{-0.10}$	[21]
IC 4329A	BL AGN	$0.7^{+1.8}_{-1.6}$	[21]
PG 0026+12	NL AGN	$2.66^{+0.49}_{-0.55}$	[21]
MRK 279	BL AGN	4.17	[12]
F 9	BL AGN	$8.3^{+2.5}_{-4.3}$	[21]
MRK 841	BL AGN	14.1	[12]
PG 1116+215	BL AGN	16.2	[23]
PG 0804+761	BL AGN	$16.3^{+1.6}_{-1.5}$	[21]
AKN 120	BL AGN	$18.7^{+4.0}_{-4.4}$	[21]
MCG−2-58-22	BL AGN	34.7	[12]
MRK 1383	BL AGN	37^{+13}_{-16}	[21]
IRAS F04250−5718	BL AGN	38.0	[12]
HE 1029-1401	BL AGN	120	[23]

The measurements of the excess variance of a red-noise process will possess a large scatter about their mean [27, see also the following section]. This scatter is, of course, reduced by averaging over many realizations. Therefore, in our analysis, light curves longer than 40 ks were subdivided into many shorter segments. This allowed us to maximize the number of variance measurements per object.

We extracted a 2–10 keV combined SIS0 and SIS1 light curve for each object. We only used light curves comprising at least 20 bins, with each bin having no fewer than 20 counts. Some light curves, having been initially extracted, contained some bins having fewer than 20 counts. In these cases, we excised bins from the light curve, on the basis of fractional exposure, so that only valid bins remained. The invalid bins could thus be removed from the light curve without introducing bias.

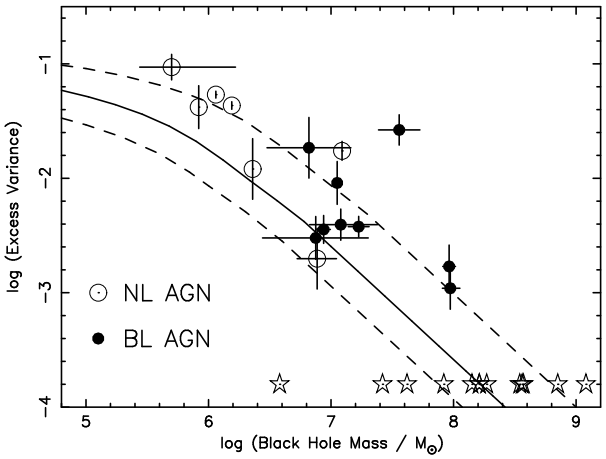

FIGURE 1. Log_{10} of excess variance versus $\log_{10}$ of black-hole mass. Open and filled circles represent NL AGNs and BL AGNs, respectively. The stars indicate the masses of those objects in which variability was not detected. The solid line shows the expected variance assuming a twice-broken power law, and the dashed lines show the range in the expected value.

There were 29 objects for which we had at least a single valid light curve segment. These objects are listed in Table 1. We determined the χ^2 corresponding to the hypothesis of a constant counting rate for each segment. We then summed all of the χ^2s and degrees-of-freedom for each object, and thereby tested whether that object exhibited variability. We detected variability in 16 objects at the 95 per cent confidence significance level (see Table 1). We are yet to determine the upper limits for those objects in which variability was not detected.

For the 8 objects having at least 5 measurements of excess variance, the uncertainty in the mean variance was measured from the observed scatter in those measurements. The standard deviation of the scatter about the mean was found to be ~ 60 per cent of the mean. We used this relation to assign uncertainties for the 8 objects having fewer than 5 variance measurements.

RESULTS, DISCUSSION AND FUTURE DIRECTIONS

A plot of $\log_{10}$ of the excess variance versus $\log_{10}$ of the black-hole mass is presented in Fig. 1. The open and filled circles indicate the NL AGNs and BL AGNs, respectively. The stars indicate the masses of the 13 objects in which we did not detect variability.

The solid line in Fig. 1 shows the expected variance assuming a twice-broken power-law. We determined this using the relation found from *RXTE* data for BLS1s [13], except that we also accounted for red-noise leak. The

dashed lines indicate the rough range of the expected variance based on the errors from the *RXTE* analysis.

The NL AGNs and BL AGNs follow roughly the same relation. This conclusion was also reached with previous analyses of *ASCA* data [11, 12]. We note again that our analysis is an improvement over the previous work because we have calculated the excess variance from light curves having nearly the same length.

The next step in our work is to include the GIS data in our analysis to improve our signal-to-noise and increase the number of valid light curves. We will also investigate the variance–mass relationship in different energy bands.

Most importantly, our future work will involve simulations similar to those used in modeling AGN power-spectra [e.g. 7]. This will allow us to account for the sampling of the light curves and, thereby, permit a robust comparison with a hypothesised universal power spectrum. Moreover, we shall quantify the extent to which the mean excess variance of each object differs from the expected variance. These residuals can then be examined against other parameters, such as mass-accretion rate. In this way, we can investigate the extent to which various parameters, other than black-hole mass, are associated with the X-ray variability.

ACKNOWLEDGMENTS

PMO acknowledges financial support from PPARC. This research has made use of the TARTARUS database, which is supported by Jane Turner and Kirpal Nandra under NASA grants NAG5-7385 and NAG5-7067.

REFERENCES

1. Marshall, N., Warwick, R. S., and Pounds, K. A., *MNRAS*, **194**, 987–1002 (1981).
2. Lawrence, A., and Papadakis, I., *ApJ*, **414**, L85–L88 (1993).
3. Green, A. R., McHardy, I. M., and Lehto, H. J., *MNRAS*, **265**, 664–680 (1993).
4. McHardy, I., *Mem. It. Astr. Soc*, **59**, 239–259 (1988).
5. Papadakis, I. E., and McHardy, I. M., *MNRAS*, **273**, 923–939 (1995).
6. McHardy, I. M., Papadakis, I. E., Uttley, P., et al., *MNRAS*, in press, [astro–ph/0311220] (2003).
7. Markowitz, A., Edelson, R., Vaughan, S., et al., *ApJ*, **593**, 96–114 (2003).
8. Nandra, K., George, I. M., Mushotzky, R. F., et al., *ApJ*, **476**, 70–82 (1997).
9. Turner, T. J., George, I. M., Nandra, K., et al., *ApJ*, **524**, 667–673 (1999).
10. Leighly, K. M., *ApJS*, **125**, 297–316 (1999).
11. Lu, Y., and Yu, Q., *MNRAS*, **324**, 653–658 (2001).
12. Bian, W., and Zhao, Y., *MNRAS*, **343**, 164–168 (2003).
13. Papadakis, I. E., *MNRAS*, in press, [astro–ph/0311016] (2003).
14. Tanaka, Y., Inoue, H., and Holt, S. S., *PASJ*, **46**, L37–L41 (1994).
15. Serlemitsos, P., Jalota, L., Soong, Y., et al., *PASJ*, **47**, 105–114 (1995).
16. Gendreau, K., *X-ray CCDs for Space Applications: Calibration, Radiation Hardness, and Use for Measuring the Spectrum of the Cosmic X-ray Background*, Ph.D. thesis, Massachusetts Institute of Technology (1995).
17. Ohashi, T., Ebisawa, K., Fukazawa, et al., *PASJ*, **48**, 157–170 (1996).
18. Turner, T. J., Nandra, K., Turcan, D., et al., "Tartarus-An ASCA AGN database," in *AIP Conf. Proc. 599: X-ray Astronomy: Stellar Endpoints, AGN, and the Diffuse X-ray Background*, 2001, pp. 991–994.
19. Shemmer, O., Uttley, P., Netzer, H., and McHardy, I. M., *MNRAS*, **343**, 1341–1347 (2003).
20. Onken, C. A., Peterson, B. M., Dietrich, M., et al., *ApJ*, **585**, 121–127 (2003).
21. Kaspi, S., Smith, P. S., Netzer, H., et al., *ApJ*, **533**, 631–649 (2000).
22. Onken, C. A., and Peterson, B. M., *ApJ*, **572**, 746–752 (2003).
23. Woo, J. H., and Urry, C. M., *ApJ*, **579**, 530–544 (2002).
24. Peterson, B. M., Wanders, I., Bertram, et al., *ApJ*, **501**, 82–93 (1998).
25. Boroson, T. A., and Green, R. F., *ApJS*, **80**, 109–135 (1992).
26. McLure, R. J., and Dunlop, J. S., *MNRAS*, **327**, 199–207 (2001).
27. Vaughan, S., Edelson, R., Warwick, R. S., et al., *MNRAS*, **345**, 1271–1284 (2003).